AUT Journal of Electrical Engineering

AUT J. Elec. Eng., 51(1) (2019) 93-100
DOI: 10.22060/eej.2018.14934.5248

Unmanned Aerial Vehicle Field Sampling and Antenna Pattern Reconstruction Using Bayesian Compressed Sensing

S. Mirzaei[1], A. Gholipour[2]

[1] School of Engineering Science, College of Engineering, University of Tehran, Tehran, Iran
[2] Department of Electrical Engineering, Shahid Beheshti University, Tehran, Iran

ABSTRACT: Antenna 3D pattern measurement can be a tedious and time-consuming task even for antennas with manageable sizes inside anechoic chambers. Performing onsite measurements by scanning the whole 4π [sr] solid angle around the antenna under test (AUT) is more complicated. In this paper, with the aim of minimum duration of the flight, a test scenario using unmanned aerial vehicles (UAV) is proposed. A practically optimal scanning strategy is presented. The suggested techniques are beneficial particularly for the case of large directive antennas. The UAV follows a predefined trajectory in the scanning windows around the AUT and reads the field strength. Then, using compressed sensing (CS) method, the antenna pattern is reconstructed. It is shown that applying Bayesian CS algorithm to the samples of field intensity gathered by UAV can efficiently reconstruct the pattern. Discrete Cosine Transform (DCT) is utilized for sparsifying the antenna patterns. Performance is evaluated by obtaining the reconstructed patterns for different antenna types. The effects of the antenna type and area of scanning are analyzed. It is shown that satisfying performance can be achieved by measuring about 50 percent of the total pattern samples. The reconstruction error of different CS implementations is computed and the superiority of Bayesian CS is illustrated.

Review History:
Received: 5 September 2018
Revised: 9 October 2018
Accepted: 10 October 2018
Available Online: 10 October 2018

Keywords:
Antenna pattern
unmanned aerial vehicle (UAV)
compressed sensing (CS)
Bayesian CS
far field measurement
field scanner

1- Introduction

The radiation pattern of an antenna under test is generally measured in anechoic chambers. This is the preferred test set up due to its good accuracy, its control over environmental conditions and being less prone to electromagnetic interference. Both near field and far field measurements may be conducted [1]. For electrically large antennas, outdoor range or compact ranges may be the choice [2, 3]. In some situations, evaluation of the electrical behavior of AUT in its operational conditions is required [4, 5]. Characterization of an antenna mounted on an aircraft or antennas in an antenna farm are some examples of these conditions. In these situations, in-situ measurements are performed.

Quadcopters and drones are unmanned aerial vehicles (UAVs) that can potentially be used for onsite measurements. Similar to the anechoic chamber test scenarios, practical UAV measurements can be performed in the near field (NF) or far field (FF) regions [6, 7].

In NF methods, the measurements are performed in the proximity of AUT [8]. Then equivalent surface currents are computed based on the measured data [9]. Knowing the equivalent surface currents, the desired FF pattern is obtained. The accuracy of the reconstructed pattern depends on the accuracy of the positioning mechanism. Normally, computing the equivalent surface currents is easier if both amplitude and phase information exist. However, in most outdoor range cases it is not practical to perform phase measurements. Therefore, only the field strength is measured and the phase information of the equivalent currents is retrieved numerically. In iterative phase retrieval techniques, the samples are collected on two or more acquisition surfaces. The spatial variation of the field distribution against distance in the AUT NF region is necessary to provide enough equations for the successful deployment of phase recovery algorithms [9]. The main drawback of the phase retrieval algorithms is their tendency to be trapped in local minima.

In FF measurement methods, the field is sampled in the Fraunhofer region. Measurements, in this case, are less prone to positioning errors. NF to FF is not required, as well. However, the FF measurements suffer longer flight paths which entail more flights.

With today's technology, cheap drones with stable navigation exist, but the flight duration, maximum tolerable weight, and battery usage are the limitations. Due to these limitations, 3D far field pattern cannot be measured by scanning the 4π [sr] solid angle around the AUT. Hence, the efficient sampling procedure is needed together with an efficient algorithm which is able to reconstruct the pattern with a minimum number of samples. It is shown that the compressed sensing method with properly selected basis functions can play this role.

Sparse signal recovery has been widely used in various areas in recent years. If we are able to find a sparse representation of the desired signal in a basis domain, we can save the resources by reconstructing the original signal from a small number of measured samples. This is the idea behind Compressed Sensing (CS) techniques [10, 11]. Many applications ranging from image reconstruction, radar imaging and target detection, sensor networks and in general, data compression methods may benefit from CS [23-30].

The CS is applied to FF samples; hence, it reconstructs the pattern from the phaseless data. Consequently, it requires

Corresponding author, E-mail:

lower computational resources compared to those methods which need to perform phase retrieval algorithms. Also, it does not trap in local minima. Here, we propose to use Bayesian CS (BCS). Bayesian approach assumes a prior probability distribution for the unknown parameters of the model. The observations are supposed to be generated from a known probability distribution conditioned on the unknown parameters. Thus, the unknown parameters' posterior probability distributions are inferred through Maximum A Posteriori (MAP) estimation. This way, instead of point estimation, a probability distribution is acquired for unknown parameters which can give us the capability to adaptively fit the model to data, select the model order or complexity and obtain the error estimation which can be exploited to optimize the model.

Bayesian version of the CS model is applied to the problem of antenna pattern reconstruction due to several benefits of Bayesian modeling mentioned above. Bayesian compressed sensing technique is used to construct the FF pattern from a small number of measurements. The performance of the Bayesian framework is studied and the results are analyzed and compared with classical CS reconstruction techniques.

The remainder of this paper is organized as follows. In section 2, the main idea of Bayesian CS is explained. In section 3, the scanning strategy of the UAV and the test scenario are described. The results of the reconstructed patterns for different antenna types are presented in section 4. In section 5, the performance of two distinct implementations of the reconstruction algorithm is explored. Some conclusive remarks are presented in section 6.

2- Sparse reconstruction techniques

Suppose that we have a data vector $\mathbf{x}_{n\times1}$ which can be sparsely represented in the Discrete Fourier Transform (DFT) basis:

$$x = \Phi s, \tag{1}$$

where $\Phi_{n\times n}$ is the DFT matrix and $\mathbf{s}_{n\times1}$ is a sparse vector with $k << n$ non-zero elements. Now we can sample the data vector $\mathbf{x}$ by the measurement matrix $\mathbf{A}_{m\times n}$ and obtain the measured vector with dimension m which is significantly smaller than the data size n:

$$y_{m\times1} = Ax = A\Phi s = \Psi s. \tag{2}$$

Here, $\Psi_{m\times n} = A\Phi$ contains the rows of the basis matrix Φ corresponding to the measured samples. Thus, the samples in $\mathbf{y}$ can be a subset of size m of the samples in $\mathbf{x}$ or a linear combination of these m samples. In a typical CS model, the observation vector $\mathbf{y}$ is affected by measurement noise, as well. The noise effect can be considered as an additive Gaussian noise vector ε with a zero-mean:

$$y = \Psi s + \varepsilon. \tag{3}$$

Our objective is to reconstruct the original data $\mathbf{x}$ from the measured samples in $\mathbf{y}$. In other words, we desire to solve the following optimization problem:

$$\hat{s} = \arg\min_{s} \left\{ \|y - \Psi s\|_2^2 + \lambda \|s\|_0 \right\}, \tag{4}$$

where $\lambda\|s\|_0$ is the regularization term imposing the sparsity to the solution. Since the above problem with l0-norm constraint is NP-hard, we simplify it by applying l1-norm instead:

$$\hat{s} = \arg\min_{s} \left\{ \|y - \Psi s\|_2^2 + \lambda \|s\|_1 \right\}. \tag{5}$$

Subsequently, the reconstructed signal $\hat{\mathbf{x}}$ can be achieved through multiplying the sparse vector $\hat{\mathbf{s}}$ by the inverse DFT matrix Φ^{-1}:

$$\hat{x} = \Phi^{-1}\hat{s}. \tag{6}$$

CS reconstruction error depends on the sparsity level of $\mathbf{X}$ and on the incoherency among the sparsity basis vectors Φ and the measurement matrix $\mathbf{A}$ [11]. It has been shown that randomly sampled matrices have low coherency with most of the representation bases, hence they can be utilized to achieve minimum reconstruction error [10, 11]. In [12, 13], some deterministic techniques are introduced to determine the sampling matrix $\mathbf{A}$.

Many approaches have been proposed in the literature to solve the above optimization problem, including linear programming algorithms, basis-pursuit, matching-pursuit, etc. [5-9].

In [19-22], compressed sensing problem is formulated in a Bayesian framework which is more effective in many aspects. Bayesian approach assumes that the elements of the vector s are random variables drawn from an assigned sparse prior distribution to impose sparsity to the solution. Therefore, the observation vector $\mathbf{y}$ is also random with conditional distribution $P(y \mid s, \Sigma_n)$ where $\sum_n$ is the noise variance. Variational Bayesian techniques or sampling Markov Chain Monte Carlo (MCMC) method can be employed to infer the unknown parameters and estimate the sparse vector s. Bayesian approach has many advantages over deterministic formulation. The main advantage is that instead of point estimation, we obtain a distribution for the unknown elements of $\mathbf{s}$ via MAP estimation which is more accurate; this can give us an estimation of the reconstruction error and help in optimizing the measurement matrix to reduce the uncertainty of the estimated sparse vector. Furthermore, noise posterior distribution can be inferred. As can be observed in the experiments, the Bayesian method outperforms other formulations in terms of the reconstruction error. Regarding the above advantages, we propose a pattern reconstruction technique based on Bayesian compressed sensing. We adopt the formulation proposed in [19] where a hierarchical form of Laplace distribution is assumed as a sparse prior imposed on $\mathbf{s}$:

$$P(\mathbf{s} \mid \lambda) = \frac{\lambda}{2}\exp\left(\frac{-\lambda}{2}\|\mathbf{s}\|_1\right), \tag{7}$$

where λ controls the sparsity level. It is obvious that choosing the Laplace prior and obtaining the MAP estimation is equivalent to l1 regularization in the non-Bayesian framework. The observation noise is supposed to be a zero-mean Gaussian with the variance of β^{-1}. Hence, the generative model of the observed vector $\mathbf{y}$ is as follows [19]:

$$P(y \mid s, \beta) = N(y \mid \Psi s, \beta^{-1}). \tag{8}$$

A Gamma prior distribution is enforced on β parameter which again imposes sparsity. Bayesian inference update equations can be found in [19].

The comparison among different CS techniques is presented in the experiments section and will exhibit the superior performance of the Bayesian method.

Different applications make use of various transforms for the purpose of sparse representation. For example, DFT matrix can be exploited as a linear transform to make the data sparse as explained above. Another common basis matrix is Discrete

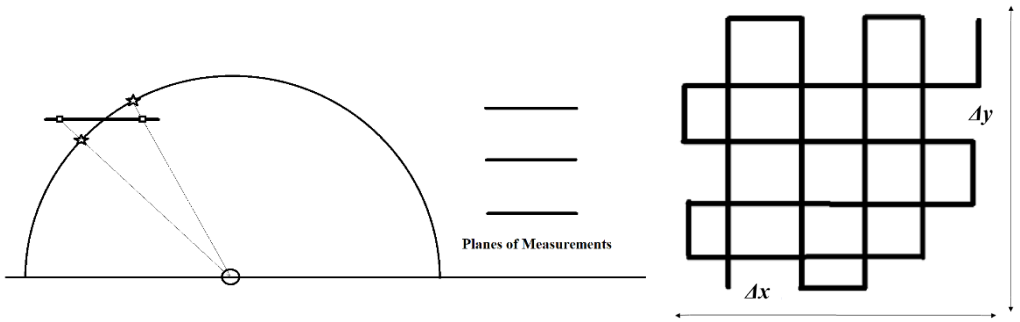

Fig. 1. (a) Scanning planes (b) The trajectory of UAV

Cosine Transform (DCT) which contains real basis functions in contrast to the DFT with complex values. Wavelet is an example of a non-linear transform which is commonly deployed for sparse representation in some applications. For the current problem of antenna pattern reconstruction, we prefer the DCT basis matrix rather than the other mentioned transforms due to its better results proven empirically.

3- Implementation

Drones are good candidates to sample the field strength in space, however, they suffer from some limitations that make their usage for antenna pattern measurements problematic. To obtain the antenna pattern, samples on the surface of a fictitious sphere around AUT in the far field should be collected. But drones are more controllable in horizontal planes rather than spherical surfaces. This makes the scanning strategy, together with the positioning system, the key factors of acquiring accurate measurements.

From electromagnetic theory it is known that in the far field, the Sommerfeld radiation condition is satisfied [1]:

$$\mathbf{E}(r,\theta,\varphi)=\mathbf{E}^0(\theta,\varphi)\frac{e^{-jkr}}{r}, \tag{9}$$

where $\mathbf{E}$ is the electric field vector and k is the wave number in free space. In our notations, vectors are indicated in boldface letters. The radiation intensity then is defined as:

$$U(\theta,\varphi)=\frac{r^2}{2\eta}\left|\mathbf{E}(r,\theta,\varphi)\right|^2=\frac{1}{2\eta}\left[\left|E_\theta^0(\theta,\varphi)\right|^2+\left|E_\varphi^0(\theta,\varphi)\right|^2\right]. \tag{10}$$

The data collection strategy is depicted in Fig. 1a and 1b. Fig. 1a shows the horizontal planes where the UAV reads the field strength and Fig. 1b illustrates the trajectory of UAV on that plane. Suppose that $\left|\mathbf{E}^m\right|^2$ is the field strength at the observation point m on nth measurement plane. With respect to the global coordinate system defined in Fig.1, the observation vector has x_m, y_m and z_m components. Correspondingly, in a spherical coordinate system this vector consists of r_m, θ_m, φ_m elements:

$$U_m(\theta_m,\varphi_m)=\frac{\left[x_m^2+y_m^2+z_m^2\right]}{2\eta}\left|\mathbf{E}_m(x_m,y_m,z_m)\right|^2. \tag{11}$$

Our goal is to reconstruct the antenna pattern from a small number of field strength measurements. The CS idea discussed in section II can be well adapted with the problem at hand. We first need to determine the strategy of scanning and data acquisition. Suppose that in each flight the drone collects samples from the sector of $\Delta x\times\Delta y$ on the horizontal plane with the height of z_m. Each point on the scanning plane can be mapped on the radiation sphere around the AUT. Equation (10) can be used to find the radiation intensity in that specific direction. Therefore, each scanning plane determines a sector of $\Delta\theta\times\Delta\varphi$ in space.

Ultimately, a matrix of collected data can be constructed. Fig 2 demonstrates the image like the representation of this matrix. The bright rectangles define the areas that are sampled by the drone during each flight. The dark areas indicate regions with no sample collected. In this example, it is supposed that we can only take samples on every 3 degrees. This means that the total number of points in Fig.2 is 121×61 where the first dimension corresponds to swiping values of φ and the second one denotes θ variations. Thus, the size of the data vector $\mathbf{x}$ to be reconstructed is 7381. As mentioned before, the trajectory of the drone in each rectangular area can be a path like the one depicted in Fig.1.

Generally, *x, y, z* components of Cartesian coordinate can be readily transferred to r,θ,φ components of spherical coordinate: $r=\sqrt{x^2+y^2+z^2},\theta=\cos^{-1}z/r,\varphi=\tan^{-1}y/x$.

The scanning planes are linearly sampled by the trajectories depicted in Fig.1b. Then, these samples are mapped on the spherical surface as shown in the left-hand side of Fig. 1. This makes the sampling on spherical coordinate non-uniform. However, these non-uniform samples in spherical coordinate are located in bright windows of Fig. 2. In other words, scanning planes defined by $\Delta x.\Delta y$ are mapped to the bright $\Delta\theta.\Delta\varphi$ windows.

The CS algorithm may be applied to this image-like representation of a filled matrix in two different ways. In the first approach, the sample values are rearranged and stacked in

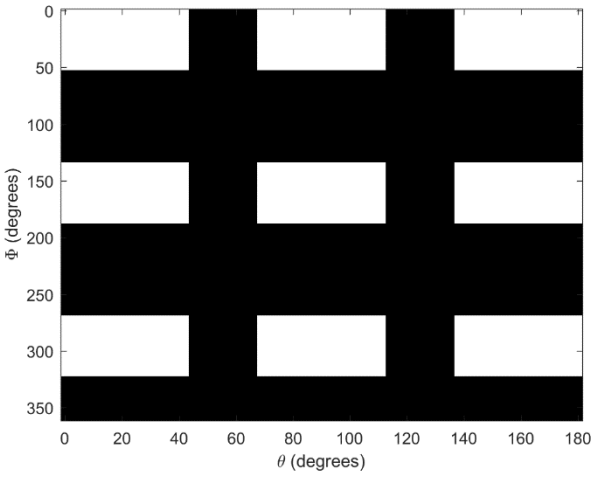

Fig. 2. Image-like representation of collected data

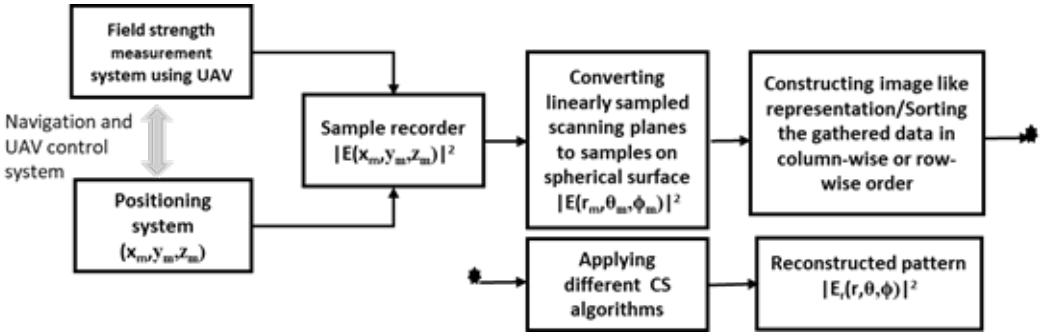

Fig. 3. Block diagram of the proposed methodology

a vector. Then, the CS algorithm tries to find the field strength at the points that have no measured data. In other words, the field strengths at the dark sectors in Fig.2 are reconstructed.

In the second approach, CS is applied to the individual columns and rows of the data matrix instead of stacking the matrix and applying the algorithm to a large vector. In the first stage, we try to estimate the missed samples at each column. Then, utilizing the reconstructed values of the previous stage, we apply CS to the individual rows of the matrix. These two steps can be executed iteratively for the purpose of diminishing the reconstruction error. It is demonstrated in section IV that the second approach can lead to a better performance in terms of the reconstruction error when the number of measurements exceeds a certain limit. The reason is that in this approach the spatial information of the data matrix is preserved in contrast to the first approach in which the adjacency information of the sampled values is disregarded by stacking the whole samples in a vector. Moreover, we generally are interested to know the pattern in specific cuts of $\varphi = const.$ or $\theta = const.$ The second approach can be used to reconstruct the pattern on that specific cut. Hence, it is not required to collect data and perform measurements in other points.

It should be noted that the order in which the missed samples are reconstructed, i.e. starting by columns or rows, depends on the known prior information about the pattern shape. For instance, when the pattern variations in an image like representation are sharper in rows, the algorithm should start with rows.

To clarify the proposed pattern measurement and reconstruction process, a flowchart of the methodology is illustrated in Fig. 3. Performance of the proposed CS technique is examined by simulating three antennas using the available commercial software packages. The proposed method can be used for measuring the radiation pattern of all types of antennas ;however, for high gain antennas or beam shaped antennas choosing the scanning planes needs more attention. Supposing that the drone is only able to get samples on the bright rectangles demonstrated in Fig.2, 2700 measured points are collected. Therefore, the CS algorithms have to find the field strength at the remaining 4681 points based on the information gathered from those 2700 samples. Referring to the notations used in section II, we first apply DCT transform to the data vector $\mathbf{x}$ to acquire the sparse vector $\mathbf{s}$, this is done by multiplying the data vector $\mathbf{x}$ by the DCT matrix. DCT is preferred over DFT since the applied CS techniques deal with real data. Subsequently, m samples out of n are measured in the vector $\mathbf{y}$. Therefore, the matrix $\mathbf{Ø}$ is made by picking *m* corresponding rows of the inverse DCT matrix. The results are reported for three antenna types. The success of applying various CS techniques as well as the impact of the number of samples on pattern reconstruction is investigated.

Bayesian CS is implemented based on the algorithm explained in section II. The Bayesian method is compared with the existing classic CS algorithms, including Matching Pursuit (MP) [7] and Stage-wise Orthogonal Matching Pursuit (StOMP) [8].

4- Experiments and results

Three types of antennas are simulated and the patterns are computed. These patterns are used as the reference data sets and are sampled based on the sampling method described in section III. Afterwards, the CS algorithms are applied to these sampled values in order to find field strengths at the remaining points of interest. The constructed patterns are compared with the reference ones and the reconstruction errors are computed. Sparsity parameter of the Laplace distribution in Eq. 7 is set to $\lambda = 2$. Hyperparameters of Gamma distribution in Eq. 8 are chosen 0.2 for shape parameter and 1 for scale parameter. The criterion of root mean square is used to calculate the error. Since the patterns are normalized, the reconstruction errors of different antenna types are comparable. Based on these reconstruction errors, successfulness of the algorithms is evaluated.

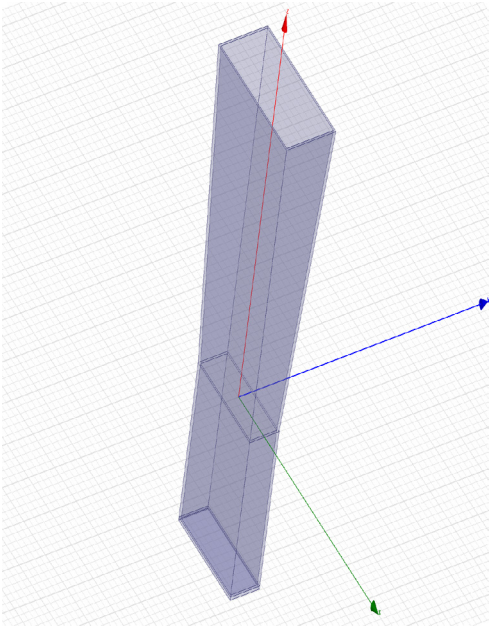

Fig. 4. The shape of the pyramidal horn antenna

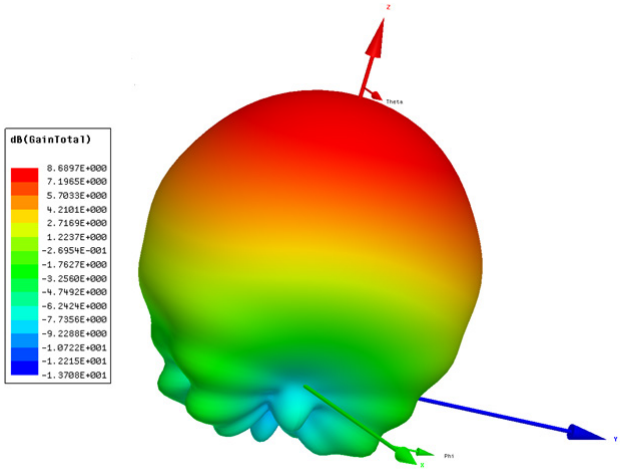

Fig. 5. 3D pattern of simulated Pyramidal Horn

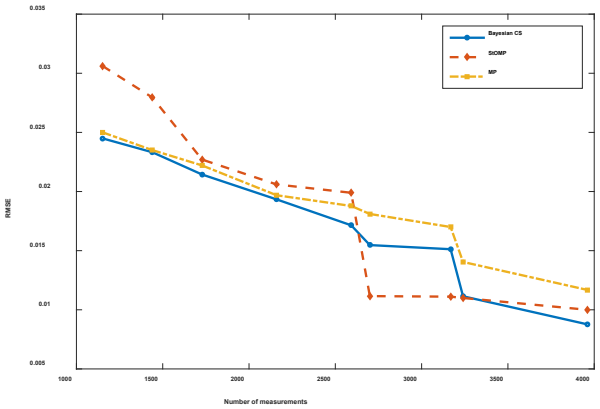

Fig. 6. RMSE error of different CS techniques applied to the horn antenna vs the number of measurements

a)Pyramidal Horn Antenna

As the first experiment, a horn antenna is studied. The geometry of this antenna is shown in Fig.4 and its 3D pattern is represented in Fig. 5. The horn antenna is an example of directive antennas. The directivity of this AUT is 9dB at 10 GHz. The Horn antenna in this example is constructed by 23.87mm×11.17mm rectangular waveguide terminated in 31.5mm×18.8mm aperture. The samples are gathered based on the scenario described in section 2. The total number of samples is 121×61.

If we need to find a pattern in a specific cut or solid angle, we can just measure the pattern at some points around that region and then find the pattern at the points in between.

Fig. 6 compares the reconstruction error of the Bayesian CS algorithm with two other classical CS techniques, i.e. MP and StOMP. For this goal, the Root Mean Square Error (RMSE) is calculated versus different numbers of measured samples. The samples were measured in 12 rectangles with specified φ_0, θ_0. To alter the number of samples, $\Delta\varphi$ and $\Delta\theta$ are varied. The graphs manifest the better performance of the Bayesian method.

For a fixed number of measured samples, the results are achieved by averaging over several arrangements corresponding to different φ_0 values for each rectangle.

Figs. 7 and 8 exhibit the reference pattern together with the reconstructed ones achieved for different numbers of measurements at two different cuts of φ=0 and φ=90 respectively. As can be observed in the figures, the main lobe is reconstructed quite well. However, the back lobe suffers more degradation mainly due to lower samples gathered from those angles.

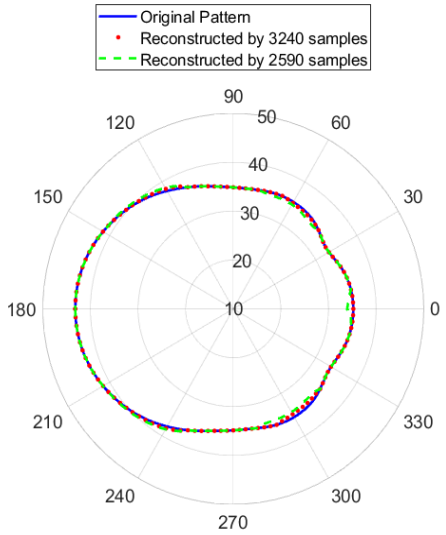

Fig. 7. H-plane cut of pyramidal horn.

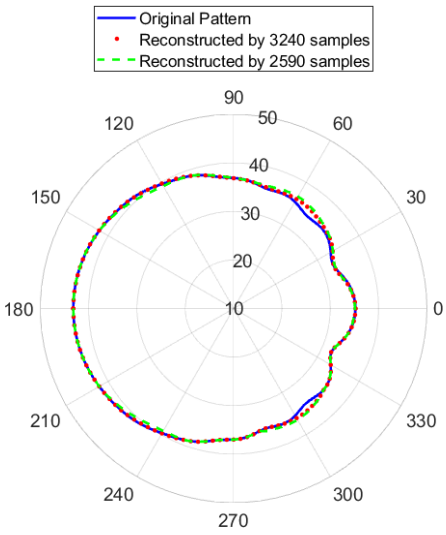

Fig. 8. E-plane cut of pyramidal horn.

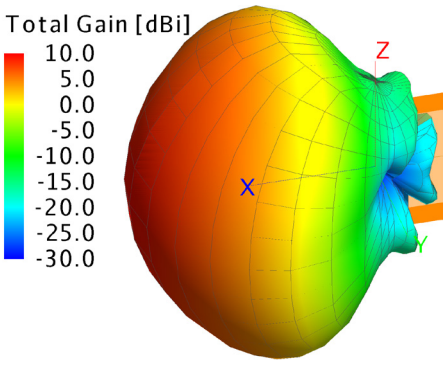

Fig. 9. 3D pattern of the simulated LPDA

b) Log-Periodic Antenna

The second example is an LPDA. The simulated 3D pattern is illustrated in Fig. 9. The total number of samples is 121×61, i.e. 7381 samples are read and fed to the CS algorithm.

Again, the performance of BCS is compared with MP and StOMP. Fig. 10 reveals that BCS is more successful in reconstructing the pattern. The outcomes of BCS algorithm are observed in Figs. 11 and 12 for the two cuts of φ = 0 and θ = 90, respectively. Very good agreement exists between the reconstructed pattern and the main pattern even for 2590 samples.

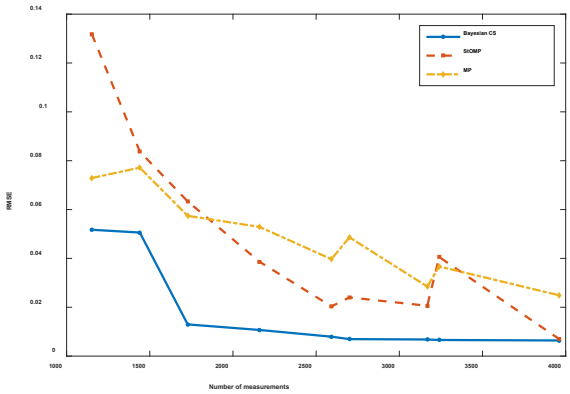

Fig. 10. RMSE error of different CS techniques applied to the LPDA antenna vs the number of measurements

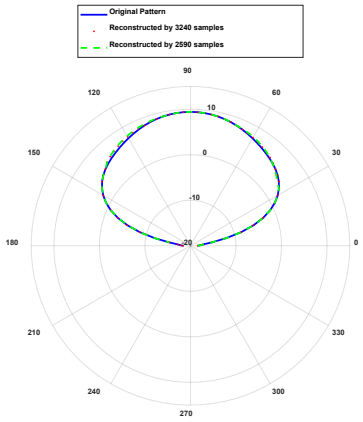

Fig. 11. 2D pattern cut of LPDA at φ = 0

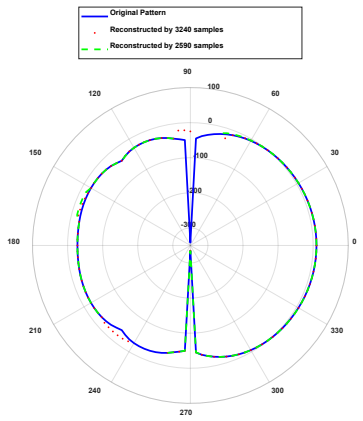

Fig. 12. 2D pattern cut of LPDA at θ = 90

c) Wired Antenna

The third example is an antenna array with three-wire antenna elements. The effect of earth on the radiation pattern is simulated by deploying the Green's function of half space in the model. FEKO has the feature of computing the Green' function of multilayer structures. This feature is used to consider the effect of earth on the AUT's radiation pattern. The permittivity $\epsilon = 5$ is supposed for the ground layer. The 3D pattern is presented in Fig.13. The range of variations of the elevation angle is $0<\theta<90$ in this case due to the presence of the ground. Therefore, the total number of samples is 121×31.

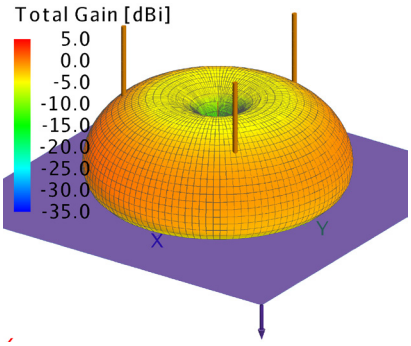

Fig. 13. 3D pattern of simulated antenna array with the antenna topology included

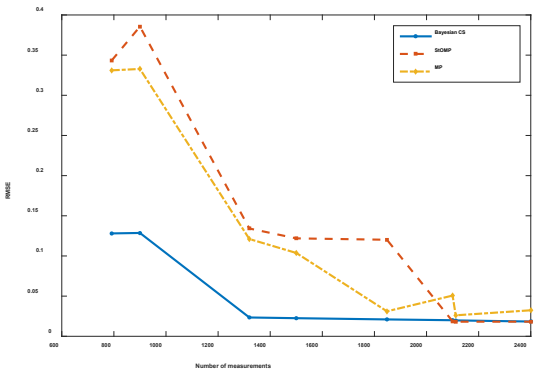

Fig. 14. RMSE error of different CS techniques applied to the wire antenna array vs the number of measurements

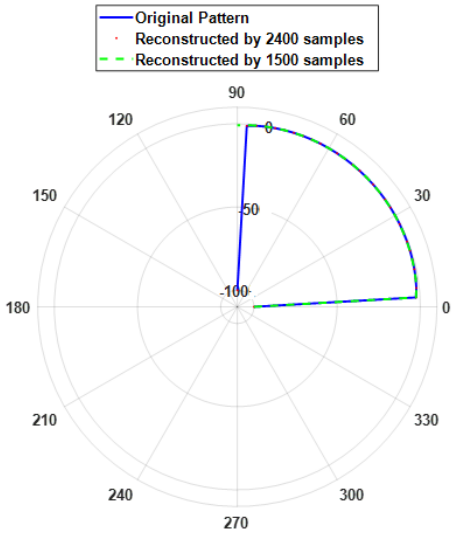

Fig. 15. 2D pattern cut of wire antenna array at φ = 0

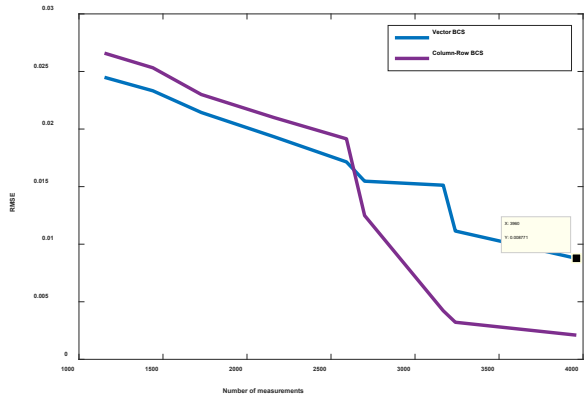

Fig. 16. RMSE error of different BCS implementations applied to the horn antenna vs the number of measurements

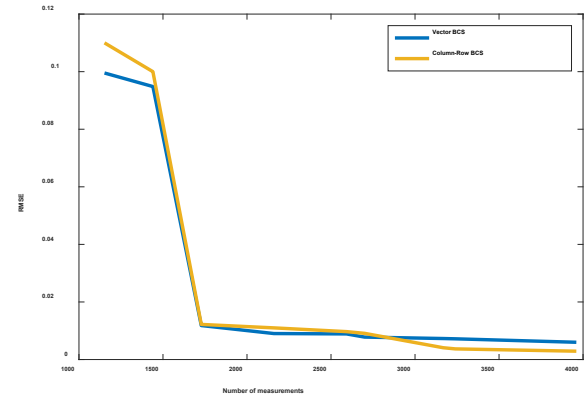

Fig. 17. RMSE error of different BCS implementations applied to the LPDA vs the number of measurements

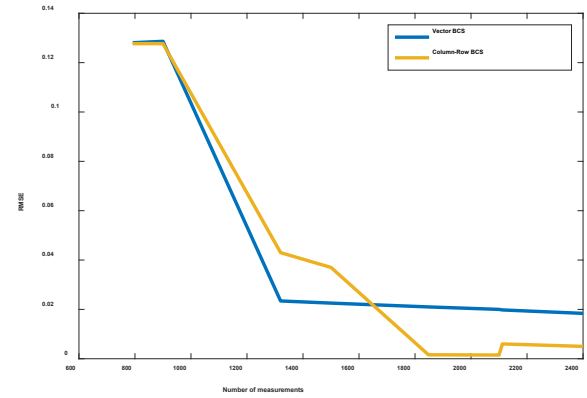

Fig. 18. RMSE error of different BCS implementations applied to the wire antenna array vs the number of measurements

The error of reconstruction is computed for different numbers of samples and reported in Fig. 14. Again, the superior performance of the BCS method is manifested. The 2D cut of the reconstructed pattern at φ = 0 is demonstrated in Fig. 15 together with the original pattern.

To examine the validity of the proposed method, several antenna types are considered for simulation. Horn antenna represents an example of high gain, directive antennas. LPDA exemplifies antennas with linear, horizontal polarization, and wire antenna array considers antenna farm problems affected by ground and the soil material property.

5- Discussion

In this section, we aim to compare the performance under two different deployment of the Bayesian CS algorithm explained in section III, i.e. the vectorial approach and column-row approach. The reconstruction error is obtained for each scenario and depicted against the number of measurements for three different antenna types discussed above.

As can be inferred from the resulted graphs (see Figs. 16 -18), the column-row method is more effective when the number of measurements is higher than about 50% of the total number of samples. This can be due to the fact that under the proposed scanning strategy, there are very small number of measured samples at some rows or columns when the total number of measurements is smaller than 50%. The better reconstruction performance achieved by the column-row approach in a higher number of measurements can be associated with maintaining the spatial information in this case.

It can be deduced that under the proposed scanning strategy, for the case where the number of measurements is higher than a threshold (here it is obtained about 50% experimentally), the column-row approach leads to a better performance in terms of the reconstruction error criterion. We can also decide about the order in which we read the data samples (First rows or first columns) exploiting the prior information about the pattern, i.e. most variations occur against θ or φ.

6- Conclusion

A pattern reconstruction technique based on Bayesian CS algorithm has been proposed. In this method, UAV was used to collect samples of field strength in the FF region of the AUT. The strategy of scanning has been described. The UAV was planned to follow the specified trajectories on horizontal planes. These sampling points were mapped on the surface of the fictitious sphere around AUT. This way, the required resources in terms of the time and costs of measurement have been reduced significantly.

It has been illustrated in the experiments section that the Bayesian CS method outperforms the conventional techniques in terms of the reconstruction error. It was also demonstrated that applying the CS algorithm to the columns and rows of the data matrix instead of the whole data vector leads to a better performance because the spatial information of the samples is preserved in the former approach.

References

[1] C. Balanis, *Antenna theory : analysis and design*, Wiley-Interscience, Hoboken, N.J., 2016.

[2] J.D. Kraus, R.J. Marhefka, *Antennas for all applications*, in, McGraw-Hill, New York, 2002.

[3] R.B. Dybdal, Communication satellite antenna testing, *IEEE Instrumentation & Measurement Magazine*, 18(3) (2015) 28-33.

[4] M. García-Fernández, Y.Á. López, A. Arboleya, B. González-Valdés, Y. Rodríguez-Vaqueiro, M.E.D.C. Gómez, F.L.-H. Andrés, Antenna diagnostics and characterization using unmanned aerial vehicles, *IEEE Access,* 5 (2017) 23563-23575.

[5] T. Schrader, J. Bredemeyer, M. Mihalachi, J. Rohde, T. Kleine-Ostmann, Concept and design of a UAS-based platform for measurements of RF signal-in-space, *Advances in Radio Science*, 14(A.) (2016) 1-9.

[6] J.-S. Suh, L. Minz, D.-H. Jung, H.-S. Kang, J.-W. Ham, S.-O. Park, Drone-based external calibration of a fully synchronized Ku-band heterodyne FMCW radar, *IEEE Transactions on Instrumentation and Measurement,* 66(8) (2017) 2189-2197.

[7] G. Virone, A.M. Lingua, M. Piras, A. Cina, F. Perini, J. Monari, F. Paonessa, O.A. Peverini, G. Addamo, R. Tascone, Antenna pattern verification system based on a micro unmanned aerial vehicle (UAV), *IEEE Antennas and Wireless Propagation Letters*, 13 (2014) 169-172.

[8] S.F. Razavi, Y. Rahmat-Samii, A new look at phaseless planar near-field measurements: limitations, simulations, measurements, and a hybrid solution, *IEEE Antennas and Propagation Magazine*, 49(2) (2007) 170-178.

[9] Y. Alvarez, F. Las-Heras, M.R. Pino, The sources reconstruction method for amplitude-only field measurements, *IEEE transactions on Antennas and Propagation,* 58(8) (2010) 2776-2781.

[10] E.J. Candes, M.B. Wakin, S.P. Boyd, Enhancing sparsity by reweighted ℓ1 minimization, *Journal of Fourier analysis and applications*, 14(5) (2008) 877-905.

[11] D.L. Donoho, Compressed sensing, *IEEE Transactions on information theory*, 52(4) (2006) 1289-1306.

[12] R.A. DeVore, Deterministic constructions of compressed sensing matrices, *Journal of complexity*, 23(4-6) (2007) 918-925.

[13] S. Gurevich, R. Hadani, N. Sochen, On some deterministic dictionaries supporting sparsity, *Journal of Fourier Analysis and Applications*, 14(5-6) (2008) 859-876.

[14] S.S. Chen, D.L. Donoho, M.A. Saunders, Atomic decomposition by basis pursuit, *SIAM review*, 43(1) (2001) 129-159.

[15] M.A. Figueiredo, R.D. Nowak, S.J. Wright, Gradient projection for sparse reconstruction: Application to compressed sensing and other inverse problems, IEEE *Journal of selected topics in signal processing*, 1(4) (2007) 586-597.

[16] J.A. Tropp, A.C. Gilbert, Signal recovery from random measurements via orthogonal matching pursuit, *IEEE Transactions on information theory*, 53(12) (2007) 4655-4666.

[17] D.L. Donoho, Y. Tsaig, I. Drori, J.-l. Starck, Sparse solution of underdetermined linear equations by stagewise orthogonal matching pursuit, submitted to, in: *IEEE Trans. on Information theory,* Citeseer, 2006.

[18] T. Blumensath, M.E. Davies, Gradient pursuits, *IEEE Transactions on Signal Processing*, 56(6) (2008) 2370-2382.

[19] S. Ji, Y. Xue, L. Carin, Bayesian compressive sensing, *IEEE Transactions on signal processing*, 56(6) (2008) 2346.

[20] S.D. Babacan, R. Molina, A.K. Katsaggelos, Bayesian compressive sensing using Laplace priors, *IEEE Transactions on Image Processing*, 19(1) (2009) 53-63.

[21] E.J. Candes, M.B. Wakin, S.P. Boyd, Enhancing sparsity by reweighted ℓ1 minimization, *Journal of Fourier analysis and applications,* 14(5) (2008) 877-905.

[22] D.P. Wipf, B.D. Rao, Sparse Bayesian learning for basis s*election, IEEE Transactions on Signal processing*, 52(8) (2004) 2153-2164.

[23] J. Wei, Y. Huang, K. Lu, L. Wang, Nonlocal low-rank-based compressed sensing for remote sensing image reconstruction, *IEEE Geoscience and Remote Sensing Letters*, 13(10) (2016) 1557-1561.

[24] D. Bi, Y. Xie, L. Ma, X. Li, X. Yang, Y.R. Zheng, Multifrequency compressed sensing for 2-D near-field synthetic aperture radar image reconstruction, *IEEE Transactions on Instrumentation and Measurement,* 66(4) (2017) 777-791.

[25] C. Li, T. Sun, K.F. Kelly, Y. Zhang, A compressive sensing and unmixing scheme for hyperspectral data processing, *IEEE Transactions on Image Processing,* 21(3) (2011) 1200-1210.

[26] A.H. Muqaibel, Efficient reformulation of image reconstruction with compressive sensing, AEU-*International Journal of Electronics and Communications,* 76 (2017) 46-51.

[27] H. Bi, C. Jiang, B. Zhang, Z. Wang, W. Hong, Radar change imaging with undersampled data based on matrix completion and bayesian compressive sensing, *IEEE Geoscience and Remote Sensing Letters*, 12(7) (2015) 1546-1550.

[28] D. Xu, L. Du, H. Liu, P. Wang, J. Yan, Y. Cong, X. Han, Compressive sensing of stepped-frequency radar based on transfer learning, *IEEE Transactions on Signal Processing*, 63(12) (2015) 3076-3087.

[29] I. Khan, D. Singh, Efficient compressive sensing based sparse channel estimation for 5G massive MIMO systems, *AEU-International Journal of Electronics and Communications*, 89 (2018) 181-190.

[30] J. Haupt, W.U. Bajwa, M. Rabbat, R. Nowak, Compressed sensing for networked data, *IEEE Signal Processing Magazine*, 25(2) (2008) 92-101.

Please cite this article using:

S. Mirzaei, A. Gholipour, Unmanned Aerial Vehicle Field Sampling and Antenna Pattern Reconstruction Using Bayesian Compressed Sensing, *AUT J. Elec. Eng.*, 51(1) (2019) 93-100.

DOI: 10.22060/eej.2018.14934.5248